jet INTL JOURNAL OF ELECTRONICS AND TELECOMMUNICATIONS, 2026, VOL. 72, NO. 3, PP. 1-8
Manuscript received October 01,2026; revised June, 2026. doi: 10.24425/ijet.2026.157949

Design massive MIMO antenna array system using Single/Double Negative (S/DNG) metamaterial unit cells for 5G sub-6 GHz base station applications

Sura Khalil Ibrahim, Mandeep Jit Singh, Mohammad Tariqul Islam, Md Shabiul Islam, Samir Salem, and Al-Bawri

Abstract—**For 5G applications, the presented paper provides a unique integrated massive multiple input-multiple output (m-MIMO) antenna system improved with the metamaterial (MTM). The compact complementary circular split-ring resonator (CSRR) with square ring ground, broad ENG (i.e., epsilon negative metamaterial) with a bandwidth of 250 MHz, and near-zero refractive index (NZRI) qualities enable the suggested system to achieve single and double negative (S/DNG) characteristics. Operating at 3.5GHz (3.37-3.62 GHz), m-MIMO antenna design consists of 4 subarrays with three layers that function inside the 5G frequency range. As opposed to conventional antennas without MTM, the antenna exhibits high port isolation between adjacent elements. Every subarray comprises eight patches, with feeding networking in the middle, partial ground on the top layer, and a full ground plan on the bottom layers. With 32 elements and a total 319 × 160 × 1.575 mm³ volume, the suggested antenna design is created and simulated. With a reflection coefficient (S11) greater than -10 dB, isolation below 39.585 dB, as well as a 10.4 dBi peak gain for every sub-array, results show that the sub-6 GHz antenna performs exceptionally well. Achieving an exceptionally low ECC (i.e., envelope correlation coefficient) of no more than 0.001 and total efficiencies in the region of >90%, along with band of 250 MHz and a 19dBi overall gain, the antenna loaded with MTM also exhibits excellent MIMO performance. The potential of the suggested antenna for cutting-edge 5G applications is highlighted by such results.**

Keywords—**article; S/DNG (single and double negative) metamaterial; Circular split-ring resonator (CSRR); m-MIMO (massive MIMO); 5G sub 6 GHz basestation**

I. Introduction

THE 5G of wireless communications technology is at the forefront due to increasing demand for high data rates. Elevating data rates to 20 Gbps and capacity, attaining ultra-low latency to 1 ms, guaranteeing high reliability, offering wide flexibility, and enhancing device-to-device communication are the main 5G communication system objectives. These goals are the focus of this technology, which tries to satisfy users' growing needs [1]–[3]. m-MIMO can be defined as a wireless access method that was researched and explored as a response to global wide band-width need in wireless communication industry. Massive MIMO is a key enabling technology for the next generation of networks, it combines antennas at receiver and transmitter in order to achieve great energy and spectral efficiency with relatively simple processing. Deploying 5G and beyond networks successfully is crucial to realizing a variety of applications regarding the intelligent sensing system, as well as to better understand massive MIMO system and addressing its underlying issues [4]–[6]. There were reports of 5G m-MIMO antenna systems for single or multiple operational bands with wide or narrow widths [7]–[10]. The Generation Partnership Project (3GPP) lately launched 3 working bands of 5-G New Radio (NR); such bands support sub-6GHz band applications in (3.30–3.80GHz), (3.30–4.20GHz), and (4.40–5GHz) span ranges, which denote N-78, N-77, and N-79, respectively [11], [12]. In addition, each nation is free to select its own 5G-demanded bands, as was previously stated. For example, China formally announced that it will use two bands: 3.30–3.60 GHz and 4.80–5.0 GHz. However, the European Union (EU) has chosen frequency band between 3.40 and 3.80 GHz for the 5G application [13], [14]. Therefore, a unique MIMO antenna system needs to be created for the purpose of covering the needed 5G N-77/N-78/N-79 bands, which isn't addressed by designs that have been provided in [15], [16], for the purpose of covering 5G operating bands for considerations of mobility. It can be difficult to design MIMO antenna types with a high degree of isolation between antenna elements, low energy consumption, cheap cost, lightweight, and small size [17]. The antenna bandwidth, which limits the use of modern wireless systems [18], [19], is one disadvantage of antenna performance. Many advanced techniques have lately been developed for avoiding such difficulties. Through adjusting the reactive impedance surface (RIS) between magnetic (PMC) and electric (PEC) conductors and surfaces, for instance, antenna radiation and bandwidth properties could be enhanced. Furthermore, it is possible to minimize the overall antenna size [20]. With the use of a 2D left-handed metamaterial (LHM) design on top (i.e., patch) and bottom (i.e., ground) sides of the dielectric substrate significantly improves the antenna performance. Because of the link between the proposed patch as well as bottom plan configuration, which results in a backward traveling wave [21], this approach gene rates capacitive-inductive properties. Nevertheless, as shown in [22], a periodic structure is added to

This work was supported by UKM.
Sura Khalil Ibrahim, Mandeep Jit Singh, Mohammad Tariqul Islamare are with Department of Electrical, Electronic and Systems Engineering, Faculty of Engineering and Built Environment, Univ. Kebangsaan Malaysia, UKM, Bangi 43600, Selangor, Malaysia (e-mail: engsurkh.18@gmail.com, {mandeep, mohmad Tariqul} @ukm.edu.my).
Md Shabiul Islam is with Faculty of Engineering, Multimedia Univ., Persiaran Multimedia, Cyberjaya, 63100 Selangor, Malaysia (e-mail: shabiul.islam@mmu.edu.my).
Samir Salem Al-Bawri is with [4]Department of Electronics & Communication Engineering, Faculty of Engineering & Petroleum, Hadhramou Univ., Al-Mukalla 50512, Hadhramout, Yemen. (e-mail: s.albawri@gmail.com).

the ground plan for passive antenna prior to the testing of temperature sensing. The bandwidth and size properties of the antenna can be greatly improved with the help of such bottom-based surface layers. With its negative refractive index, permittivity, and permeability, among other typical features, meta-material (MTM) is an artificial medium that can be utilized for a broad range of applications, such as absorbers [23], bio-sensing [24], microwave- imaging [25], antennas [26], MTM coding [27], meta-material lensing [28], terahertz MTM [29], and microwave devices such as WiMAX, GPS-5 [30]. It is done in [31], using a negative index MTM that is made of extended beams encased in a plate. In [32], [33], a 3D acoustic MTM is developed to produce bandgap at deep sound attenuation site that could be utilized as acoustic filter for the cancellation of noise. Various properties of such MTMs have been observed at specific frequency bands of interest, contingent on fixed composition of structure as well as the geometrical layout of the array. Thus, MTMs that emphasize size and many working frequencies tuned by various inputs including mechanical, optical, or electrical signals are becoming more and more popular. In [34], a hexagonal Gap linked split-ring resonator-based metamaterial covering S and X bands is constructed. Its size is (10 × 10) mm2. Open delta-shaped ENG MTM is reported to exhibit a triple-band response [35]. Moreover, a π-shaped CSRR that is coupled with metal inclusion has been designed and reported in [36], for micro-wave applications at S, C, and X-bands. The performance regarding antennas in terms of isolation, gain, band-width, patterns of radiation, etc., was confirmed in order to enhance with MTM unit cell. Because it has the capacity to modify the antenna radiator as well as the current distribution patch. On the other hand, permittivity (ε) and permeability (μ) have both experienced negative real value characteristics, and obtained refractive index (NRI) [37], [38]. Nonetheless, research was applied in a metamaterial with an NZRI feature to enhance the antenna's overall performance in particular bands, such as X bands and MTM [39]. Furthermore, to reduce the coupling between array elements, different kinds of MTMs are employed [40], [41]. For miniaturized MIMO antenna elements, however, the previously proposed techniques for decoupling are difficult to construct and implement. This research increases isolation between antenna elements by the use of a sequence of small SRRs as resonators, in contrast to traditional antenna arrays. A MIMO design with no array mode that used a multi-mode at each one of the elements (i.e., beam steering) was presented in a small number of publications. [42], describes the operation of 128 elements at 2.4 GHz along a 9-faced polyhedron ring. This was achieved by creating three modes per element using a patch that was developed. The first mode had a bandwidth of 238 MHz, the second mode had a gain of approximately 6.50 dBi, and the third mode had a gain of 1.21 dBi with a bandwidth of 102 MHz. Conversely, an array of ENG/DNG MTM is integrated with 32-element-based m-MIMO antenna system. A distinctive symmetric split-ring resonator (SSRR) MTM unit cell represents the SSRR MTM unit cell. With a 19.5 dBi overall gain, it possesses a significant negative index with more than 1GHz band-width for the ENG and negative real value characteristic of NZRI in a 3.1GHz to 4.2GHz range [43].

In order to accommodate a potential 5G base station (BS) with band of 250MHz, this research presents a high-isolation massive MIMO antenna with 32 elements, which could be covering 3.37-3.62 GHz. For supporting the operational working principle of the proposed design, which has been based upon epsilon negative and NZRI properties, an analysis of distinctive S/DNG/NZRI MTM unit cell has also been carried out. These properties have been designed for the simultaneous improvement of isolation as well as overall performance of MIMO antenna system. The suggested MTM is composed of 8-compact square-shaped splattered parts. The suggested metamaterial-based technology permits significant de-coupling of as high as 20 dB between the suggested radiating sub-MIMO antenna elements and small array elements with ECC < 0.001. This is on the contrary with conventional isolation techniques. The proposed antenna exhibits low mutual coupling and a fractional BW. Table I lists a comparison between antennas that have previously been described in the literature and the suggested MIMO antenna that has been loaded with the unique MTM.

II. Design of M-MIMO Array Antenna System

A. (S/DNG) Metamaterial Unit Cells

The metamaterial consists of two CSRRs with slotted square element in background and 2-parallel rectangular Cu elements in front of the design. In the little ring, copper structure's center is a line segment that has tunable properties. The design provides a transmission coefficient resonance S21 at 3.5GHz and a considerable operational frequency band of 220 MHz. As seen in Fig 1a, the metamaterial is composed of a Rogers 5880RT substrate and has overall dimensions of 9 × 9 mm^2.

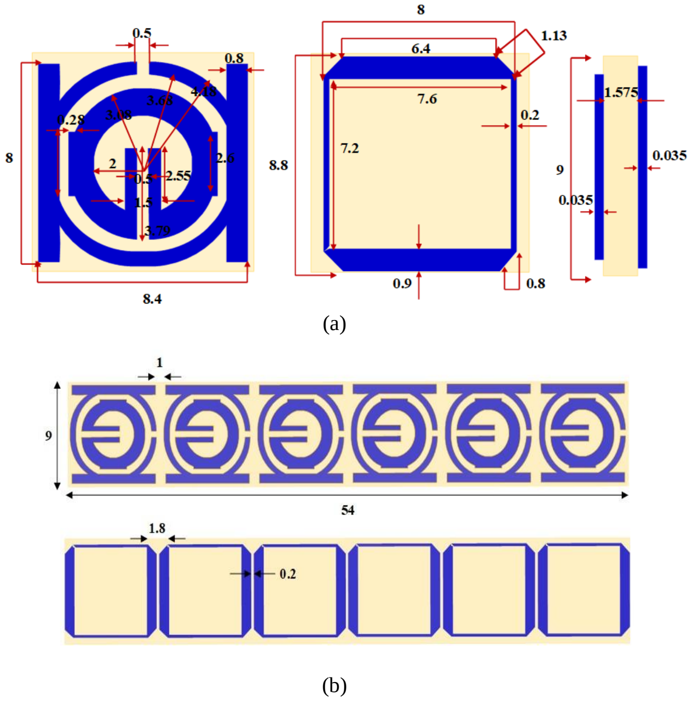

Fig. 1. S/DNG unit cell structure: (a) unit cell geometry, (b) 1 × 6 MTM unit cell array at top and bottom, respectively [49]

Table I

COMPARING THE SUGGESTED PERFORMANCE WITH PUBLISHED STATE-OF -ART PERFORMANCE.

Refs.	MIMO model	Size (mm^3)	BW (GHz)	Isolation (dB)	ECC	Eff. (%)	Gain (dB)	Techniques
[44]	4 × 8	184 × 340 × 3.15	3.4–3.65	< − 35	< 0.0001	> 95	> 19.5	Epsilon negative MTM and NZRI (ENG/ ZRI/DNG) technique characteristics were utilized for high isolation between elements and for increasing the gain.
[45]	8 × 8	560 × 560 × 266	5–6	< − 20	< 0.0035	-	> 20	Wave control has been accomplished through the changing of phase shifting distribution regarding incident waves, utilizing a meta-surface-based plane.
[46]	12 × 1	166 × 75 × 0.8	3.34–3.87	− 15	< 0.012	< 92	< 10	2-identical tapered micro-strip line fed associated with the T-shape ground were utilized for enhancing the isolation and bandwidth.
[47]	4 × 4	200 × 200 × 32	2.8–5	− 27	-	-	7.63	Dipole elements with a chamfered designed aerial bowtie in a rectangular orientation that is fed by two coaxial cables.
[48]	3 × 6	226.8 × 148.2 × 8	4–4.7	− 20	-	92	16	Channel correlation influence was investigated on the indoor wide-band massive MIMO for reducing size as well as mutual coupling.
This work	4 × 8	319×160× 1.575	3.37-3.62	< − 20	< 0.0012	>90	19	Single and double negative MTM with NZRI (S/DNG/NZRI) method characteristics were utilized for good isolation and gain.

Additionally, [49] demonstrated broad-range achievement, single/double-negative (S/DNG) equivalent circuit, negative permittivity, refractive index, and near-zero permeability qualities in 2 (z & x) primary axes of wave propagation. Fig 1b, shows a prototype of an array of (1x 6) unit cells. On top and bottom of the same substrate, in the vertical x-axis direction, DNG and SNG are formed, with a distance of 1 mm and 0.2 mm between each pair of units.

B. *Single Port Subarray*

A configuration with a single subarray design consists of 2x4 patches fed by one port and constructed on 2-dielectric layers, including three copper layers. The created feeding network (FN) is situated at middle layer, with a small partial plate in top layer, and the printed patch elements are used in top layer. An all-inclusive reference for the antenna patches as well as feeding network will be the bottom layer. Also, vias with a 1.32 mm diameter have been employed as probe feeding between the radiator elements and the FN. Roger 5880 substrates with a 2.20 dielectric constant, 0.00090 loss tangent, and 1.575mm thickness are utilized. The suggested design's side layout is depicted in Fig.2. The single port subarray's bottom and top layers with their dimensions are shown in Fig.3 and Table II.

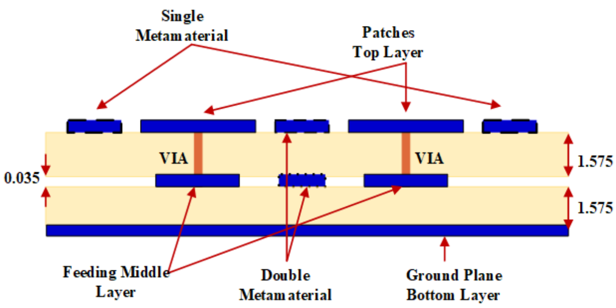

Fig. 2. Side layout of proposed design.

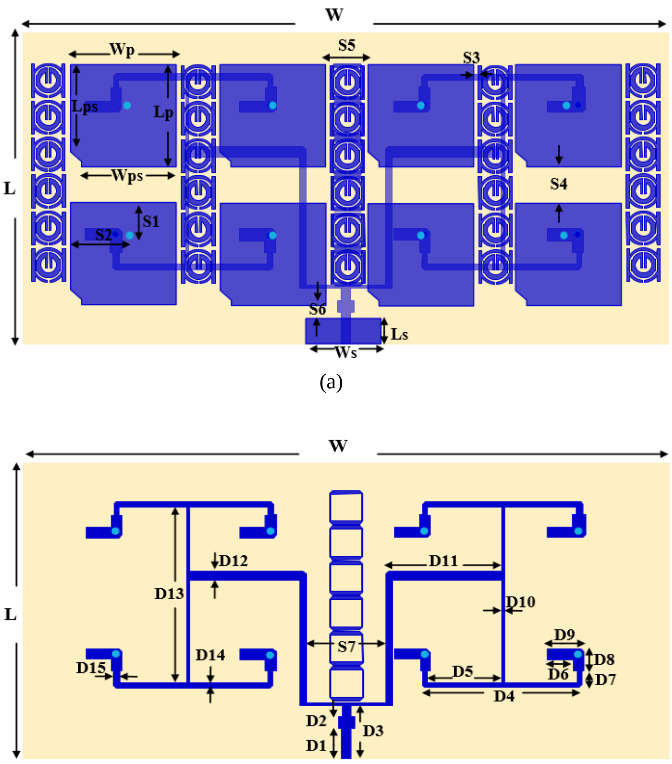

(b)

Fig. 3. The dimensions of a single-port (subarray) feeding network for (2×4) subarray antennas; (a) top layer with (2 x 4) patches, (b) bottom layer with feeding network.

TABLE II
Design parameters of proposed (2×4) subarray Antenna

Parameters	Dimensions (mm)	Parameters	Dimensions (mm)
W	165	D1	8.18
L	80	D2	2.6
Wp	28	D3	13.96
Lp	26	D4	39.6
Wps	25	D5	18
Lps	25.2	D6	6.5
Ws	20	D7	4.26
Ls	5	D8	6
S1	9.1	D9	9.11
S2	14	D10	0.68
S3	1	D11	28.66
S4	8.3	D12	2.61
S5	10.4	D13	46.3
S6	3.3	D14	1.45
S7	20	D15	1.48

C. *4-Port Subarrays*

Broadband side of 4-port (32 elements) m-MIMO antenna system loaded with meta-material with their dimensions has been shown in Fig. 4, and Table III.

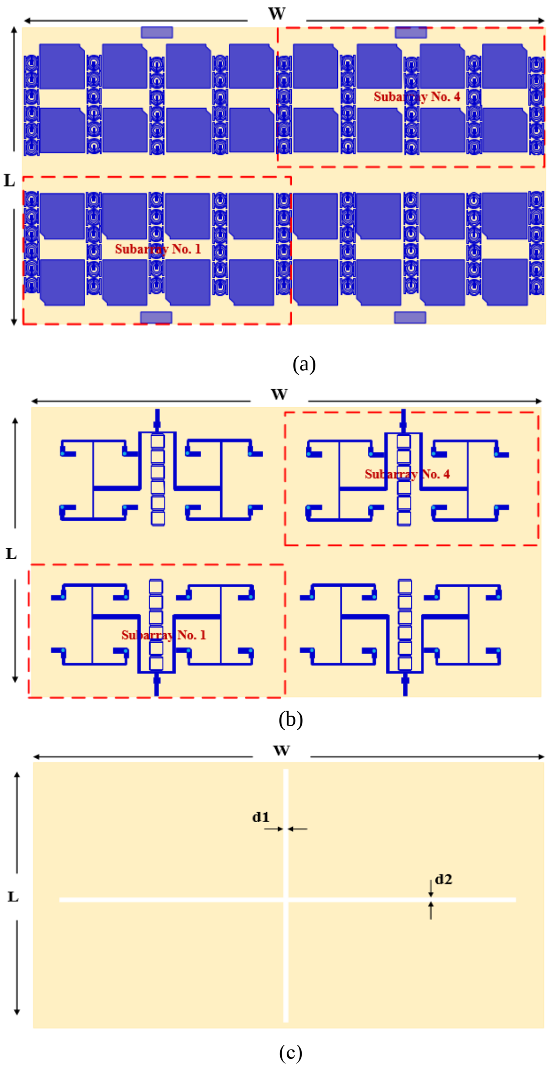

Fig. 4. A (4×8) m-MIMO array with 32-elements/4-ports of slotted microstrip patch subarray as: (a) front view; (b) 4-ports of proximity-coupled feeding network; and (c) back view.

TABLE III
Design parameters of proposed m-MIMO (4×8) array Antenna

Parameters	Dimensions (mm)	Parameters	Dimensions (mm)
W	319	d1	0.5
L	160	d2	0.5

III. RESULTS AND DISCUSSION

Simulated reflection coefficients (Sii) for each port are displayed in Fig (5), where (i = 1, 2, 3, and 4). For each subarray, the simulated obtained bands in the 3–4 GHz frequency span are 250 MHz, respectively. In addition to a large BW, Fig (6) illustrates that high isolation is achieved for each of the two adjacent ports. The decoupling effect of MTM results in a minimal degree of coupling between ports of –19.583 in the band of interest, meaning that the energy of the radiation from each of the two nearby elements is weakly coupled. The result is that in the band of interest, the adjacent subarrays are well decoupled. Additionally, displayed are cross-band coupling coefficients that are measured between 3GHz and 4GHz.

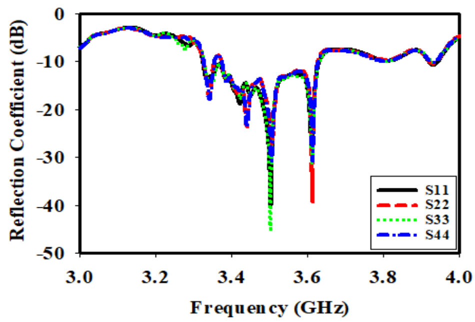

Fig. 5. Reflection coefficient for ports 1–4.

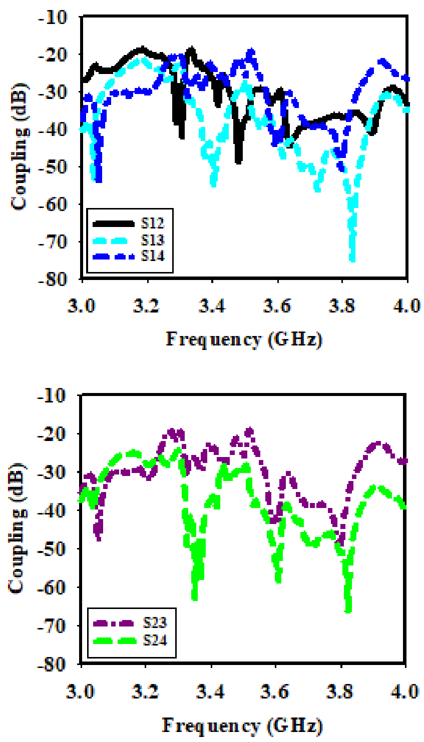

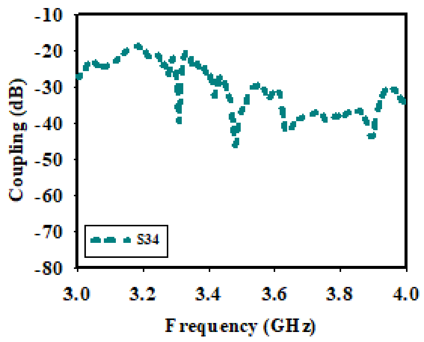

Fig. 6. Simulated coupling between each adjacent port.

The MIMO diversity performance of the suggested antenna is assessed using the ECC (Envelope Correlation Coefficient). The radiation patterns of the ports must be semi-orthogonal or orthogonal to one another in order to guarantee MIMO array mode operation. The fundamental metric for assessing correlation level between different ports is ECC [50]. With the help of the complicated electric field patterns and the learned formula, the ECC between adjacent sub-arrays is calculated.

$$\rho_{ij} = \frac{-\sum_{n-1}^{N} S_{ni}^{*} S_{nj}}{\sqrt{(1-\sum_{n-1}^{N}|S_{ni}|^{2})(1-\sum_{n-1}^{N}|S_{nj}|^{2}}} \qquad (1)$$

Where ρij represents correlation between the elements *i* & *j*, *Sni* & *Snj* are S-parameters between every one of the *n* various ports and elements *i* & *j* of the MIMO antenna system.

As shown in Fig (7), the estimated ECC of suggested MIMO antenna array in Sub 6GHz band-width for 5G at 3.5GHz is less than 0.001. Because of this, the aforementioned result shows that there is little correlation between the two antenna ports, showing excellent diversity performance. Because of the pattern of continuous radiation and high port-to-port isolation, all ECCs are less than 0.001, meeting typical ECC requirements of 0.3 in base station approaches.

Moreover, Figures (7. c) and (8.d) demonstrate effects of MTM on results of ECC. Diversity gain can be calculated with the use of the DG = 10 x$\sqrt{1 - ECC^2}$, and significant value of the diversity gain that had been achieved is 9.9 dB, as depicted in Figures (8a) and (8b) for the ports 1 to 4. For the optimal m-MIMO antenna diversity gain performance, it has to approximate to 10dB. For sub-array ports, maximal gain that has been realized is between 6 and 11.6dBi within multi-band of interest, as can be seen from Figure (9), which satisfies Figure (5) Reflection coefficient for four ports.

The suggested antenna is suitable for 5G communication since it meets functional criteria of the application of the base station. In addition to each subarray's high gain, a 19 dBi broadside gain is realized. The normalized 3.5 GHz radiation patterns of suggested antenna elements for each one of the excited ports are shown in Figure (10).

The components of the co-polarization are rather stable as a result of the effect of isolation, which can be seen from Figure (10), 2-D radiation patterns of the suggested m-MIMO antenna have been simulated in E-plane at yz within Ø = 90°, while θ = 90° in xy direction (H-plane). Far-field characteristics have indicated super directional broad-side main beam at the yz planes for the 1–4 ports; in the case where port 1 is excited, the rest of the sub-array ports become reflectors. None-the-less, a nearly omni-directional occurs in xy-plane. Additionally, the results of simulation are noticeable and in agreement.

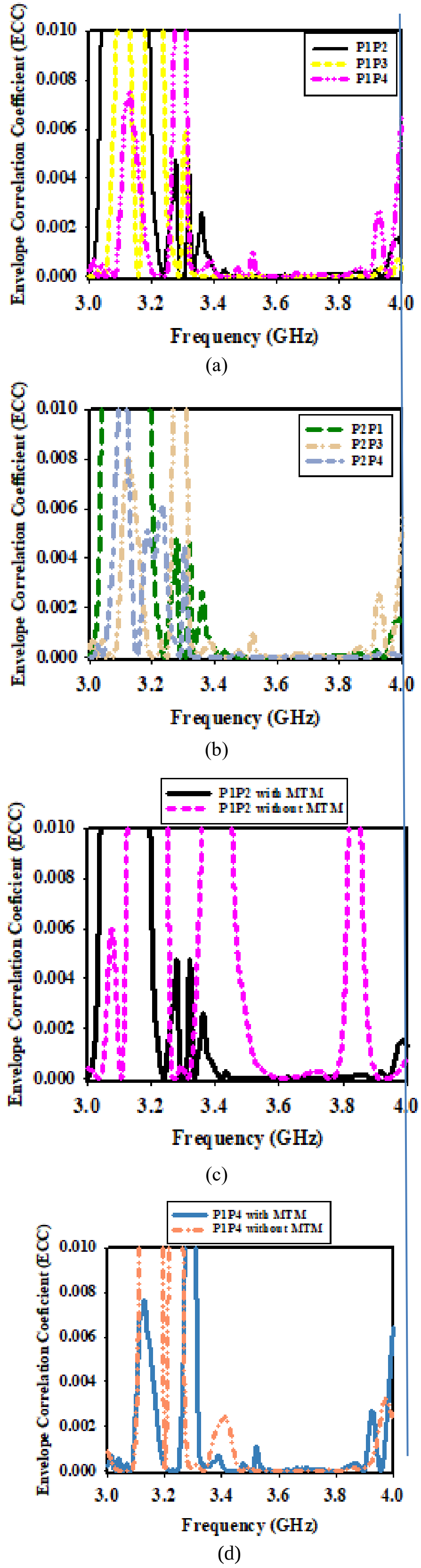

Fig. 7. The ECC of the proposed m-MIMO antenna: (a, b) Port 1, 2, 3, 4, (c, d) Port 1, 2, 4 with and with no MTM.

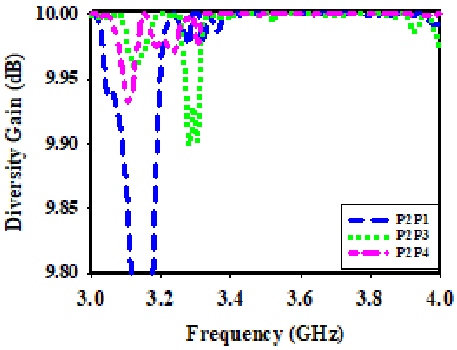

(a)

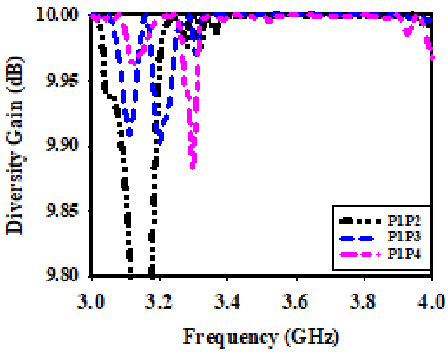

(b)

Fig. 8. Diversity gain of presented m-MIMO antenna: (a) Port 1, 2, 3, 4, (b) Port 1, 2, 4.

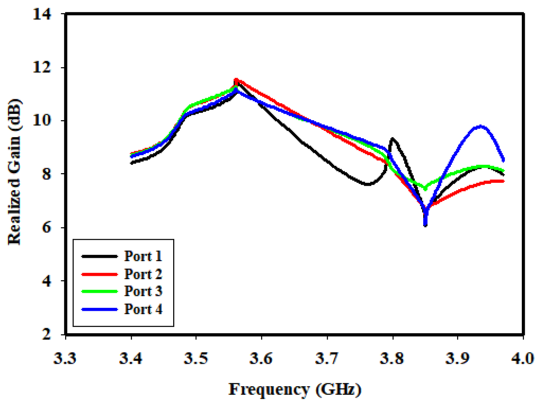

Fig. 9. Maximum realized gain of the m-MIMO array antennas.

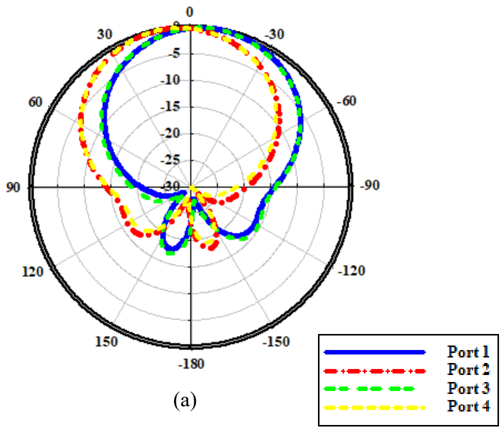

(a)

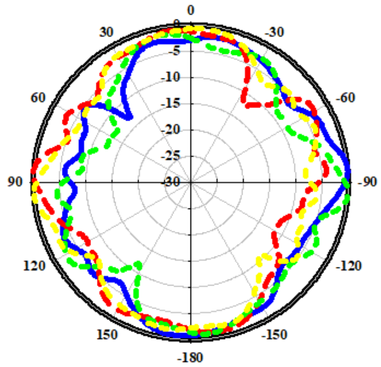

(b)

Fig. 10. Normalized radiation patterns at 3.5GHz for suggested planes at (a) YZ (Ø = 90º), (b) XY (θ = 90º).

IV. CONCLUSION

The present study offers an array of the S/DNG MTM that have been integrated into a 32-element m-MIMO array antenna system for 5-G base stations. The unit cell is a unique CSRR MTM unit cell, which is made up of slotted square element in background and 2 parallel rectangular copper elements in front of the design. The design provides transmission coefficient S21 resonance at 3.5GHz and a considerable operational frequency band of 250 MHz. On one side panel, four sub-arrays have been arranged with full as well as partial grounds on top and back of both layers, respectively. In band of interest at 3.5GHz, minimal measured gain is 6dBi, while minimal measured BW has been obtained at 250 MHz. However, the realized efficiency is defined as >90%. Good isolation is accomplished even in the case where both antennas are rather close, and the maximal ECC performance between ports is 0.001. Finally, the presented m-MIMO array, consisting of 32 compact elements, performs well in general and in isolation, making it one of the viable options for the 5G sub-6GHz BS applications.

REFERENCES

[1] Abdaljabar, J. S., Al-Hindawi, A. & Kabalan, K. Y. A Comprehensive Study of Massive MIMO Antenna Arrays in the Next Generation of Communication Networks. *Int. J. Commun. Antenna Propag. (IRECAP).* 11, 5 (2021).

[2] Pant, M. & Malviya, L. Design, developments, and applications of 5G antennas: a review. *Int. J. Microw. Wirel. Technol.* 1–27; doi: 10.1017/S1759078722000095 (2022).

[3] Zada, M. I., Shah, A., & Yoo, H. Integration of Sub-6-GHz and mm-Wave Bands with a Large Frequency Ratio for Future 5G MIMO Applications. *IEEE Access*. 9, 11241–11251;

doi: 10.1109/ACCESS.2021.3051066 (2021).

[4] Ibrahim, S. K. et al. Design, Challenges and Developments for 5G Massive MIMO Antenna Systems at Sub 6-GHz Band: A Review. *Nanomaterials*. 13, 3; doi: 10.3390/nano13030520 (2023).

[5] Kumar, S., Dixit, A. S., Malekar, R. R., Raut, H. D. & Shevada, L. K. Fifth generation antennas: A comprehensive review of design and performance enhancement techniques. *IEEE Access*. 8, 163568–163593; doi: 10.1109/ACCESS.2020.3020952 (2020).

[6] Hussain, R. & Sharawi, M. S. 5G MIMO Antenna Designs for Base Station and User Equipment: Some recent developments and trends. *IEEE Antennas Propag. Mag.* 64, 3, 95–107; doi: 10.1109/MAP.2021.3089983 (2022).

[7] Jaglan, N., Gupta, S. D. & Sharawi, M. S. 18 Element Massive MIMO/Diversity 5G Smartphones Antenna Design for Sub-6 GHz LTE

Bands 42/43 Applications. *IEEE Open J. Antennas Propag.* 2, 533–545; doi: 10.1109/OJAP.2021.3074290 (2021).

[8] Zhao, A. & Ren, Z. Wideband MIMO antenna systems based on coupled-loop antenna for 5G N77/N78/N79 applications in mobile terminals. *IEEE Access*. 7, 93761–93771;

doi: 10.1109/ACCESS.2019.2913466 (2019).

[9] Shabbir, T. et al. 16-Port non-planar mimo antenna system with near-zero-index (nzi) metamaterial decoupling structure for 5g applications. *IEEE Access*. 8, 16, 157946–157958;

doi: 10.1109/ACCESS.2020.3020282 (2020).

[10] Sun, L., Li, Y., Zhang, Z. & Feng, Z. Wideband 5G MIMO Antenna with Integrated Orthogonal-Mode Dual-Antenna Pairs for Metal-Rimmed Smartphones. *IEEE Trans. Antennas Propag*. 68, 4, 2494–2503; doi: 10.1109/TAP.2019.2948707 (2020).

[11] Huawei. 5G Spectrum. Preprint at https://www-file.huawei.com/-/media/corporate/pdf/public-policy/public_policy_position_5g_spectrum_2018.pdf?la=en (2018).

[12] Scarlet, D. The 5G Evolution. *J. Chem. Inf. Model.* 53, 9, 1689–1699 (2020).

[13] Parvini, M. et al. Spectrum Sharing Schemes From 4G to 5G and Beyond: Protocol Flow, Regulation, Ecosystem, Economic. *IEEE Open J. Commun. Soc.* 4, 464–517; doi: 10.1109/OJCOMS.2023.3238569 (2023).

[14] Sufian, M. A., Hussain, N., Askari, H., Park, S. G., Shin, K. S. & Kim, N. Isolation Enhancement of a Metasurface-Based MIMO Antenna Using Slots and Shorting Pins. *IEEE Access*. 9, 73533–73543; doi: 10.1109/ACCESS.2021.3079965 (2021).

[15] Li, Y., Sim, C. Y. D., Luo, Y. & Yang, G. 12-Port 5G Massive MIMO Antenna Array in Sub-6GHz Mobile Handset for LTE Bands 42/43/46 Applications. *IEEE Access*. 6, 344–354;

doi: 10.1109/ACCESS.2017.2763161 (2017).

[16] J. Huang, G. Dong, J. Cai, H. Li, and G. Liu, "A quad-port dual-band mimo antenna array for 5g smartphone applications," *Electron.* 10, 5, 1–9; doi: 10.3390/electronics10050542 (2021).

[17] Badi, S. K. & Acharya, O. P. Isolation Enhancement in MIMO with Low Space Diversity for 5G/WLAN Applications. *Int. Conf. Adv. Commun. Technol. Signal Process. ACTS 2020,* 1-5; doi: 10.1109/ACTS49415.2020.9350441 (2020).

[18] Ibrahim, S. K., Al-Bawri, S. S., Singh, M. J., Hamid Ibrahim, H. & Islam, M. T. A. High Gain and Low Cross-Polarization Compact Slotted Patch Antenna for 5G Wireless Communication Applications. *Int. Conf. Sp. Sci. Commun. Iconsp.* 161–166; doi: 10.1109/IconSpace53224.2021.9768679 (2021).

[19] Ibrahim, S. K. & Jebur, Z. T. A High Gain Compact Rectangular Patch Antenna For 5G Applications. *2021 Int. Conf. Commun. Inf. Technol.* 156–160; doi: 10.1109/icict52195.2021.9568415 (2021).

[20] Meng, F., Liu, Y. & Sharma, S. K. A miniaturized patch antenna with enhanced bandwidth by using reactive impedance surface ground and coplanar parasitic patches. *Int. J. RF Microw. Comput. Eng.* 30, 7, 1–10; doi: 10.1002/mmce.22225 (2020).

[21] Al-bawri, S. S. et al. Compact ultra-wideband monopole antenna loaded with metamaterial. *Sensors (Switzerland)*. 20, 3, 1–16; doi: 10.3390/s20030796 (2020).

[22] Yao, J., Mbanya Tchafa, F., Jain, A., Tjuatja, S. & Huang, H. Far-Field Interrogation of Microstrip Patch Antenna for Temperature Sensing Without Electronics. *IEEE Sens. J.* 16, 19, 7053–7060; doi: 10.1109/JSEN.2016.2597739 (2016).

[23] Zhong, M. Design and measurement of a narrow band metamaterial absorber in terahertz range. *Opt. Mater. (Amst).* 100, 109712; doi: 10.1016/j.optmat.2020.109712 (2019).

[24] Xu, W. et al. Terahertz biosensing with a graphene-metamaterial heterostructure platform. *Carbon N. Y.* 141, 247–252; doi: 10.1016/j.carbon.2018.09.050 (2019).

[25] Razzicchia, E., Sotiriou, I., Cano-Garcia, H., Kallos, E., Palikaras, G. & Kosmas, P. Feasibility study of enhancing microwave brain imaging using metamaterials. *Sensors (Switzerland)*. 19, 24; doi: 10.3390/s19245472 (2019).

[26] Li, C., Jiang, T., He, Q. & Peng, Z. Stiffness-mass-coding metamaterial with broadband tunability for low-frequency vibration isolation. *J. Sound Vib.* 489; doi: 10.1016/j.jsv.2020.115685 (2020).

[27] Wang, B. X., Tang, C., Niu, Q., He, Y. & Chen, R. A broadband terahertz metamaterial absorber enabled by the simple design of a rectangular-shaped resonator with an elongated slot. *Nanoscale Adv.*1, 9, 3621–3625; doi: 10.1039/c9na00385a (2019).

[28] Lv, J., Zhou, M., Gu, Q., Jiang, X., Ying, Y., & Si, G. Metamaterial lensing devices. *Molecules*. 24, 13; doi: 10.3390/molecules24132460 (2019).

[29] Wang, B. X., He, Y., Lou, P. & Xing, W. Design of a dual-band terahertz metamaterial absorber using two identical square patches for sensing application. *Nanoscale Adv.* 2, 2, 763–769; doi: 10.1039/c9na00770a (2020).

[30] Geetharamani, G. & Aathmanesan, T. Design of Metamaterial Antenna for 2.4 GHz WiFi Applications. *Wirel. Pers. Commun.* 113, 4, 2289–2300; doi: 10.1007/s11277-020-07324-z (2020).

[31] Lott, M., Roux, P., Rupin, M., Colquitt, D., & Colombi, A. Negative index metamaterial through multi-wave interactions: numerical proof of the concept of low-frequency Lamb-wave multiplexing. *Sci. Rep.* 11, 1, 1–8; doi: 10.1038/s41598-020-79572-9 (2021).

[32] Casarini, C., Windmill, J. F. C. & Jackson, J. C. 3D printed small-scale acoustic metamaterials based on Helmholtz resonators with tuned overtones. *Proc. IEEE Sensors*. 1–3; doi: 10.1109/ICSENS.2017.8234381 (2017).

[33] Gao, N., Zhang, Z., Deng, J., Guo, X., Cheng, B. & Hou, H. Acoustic Metamaterials for Noise Reduction: A Review. *Adv. Mater. Technol.* 7, 6; doi: 10.1002/admt.202100698 (2022).

[34] Shahidul Islam, M., Samsuzzaman, M., Beng, G. K., Misran, N., Amin, N. & Islam, M. T. A gap coupled hexagonal split ring resonator based metamaterial for S-band and X-band microwave applications. *IEEE Access*. 8, 68239–68253; doi: 10.1109/ACCESS.2020.2985845 (2020).

[35] Marathe, D. & Kulat, K. A Compact Triple-Band Negative Permittivity Metamaterial for C, X-Band Applications. *Int. J. Antennas Propag.* 2017; doi: 10.1155/2017/7515264 (2017).

[36] Islam, M. R., Samsuzzaman, M., Misran, N., Beng, G. K. & Islam, M. T. A tri-band left-handed meta-atom enabled designed with high effective medium ratio for microwave based applications. *Results Phys.* 17, 103032; doi: 10.1016/j.rinp.2020.103032 (2020).

[37] Al-bawri, S. S., Islam, S., Wong, H. Y. & Jamlos, M. F. Bandwidth and Gain Enhancement of Quad-Band CPW-Fed Antenna for Wireless Applications. *Sensors*. 20, 2, 1–14 (2020).

[38] Shabbir, T., Saleem, R., Al-Bawri, S. S., Shafique, M. F. & Islam, M. T. Eight-Port Metamaterial Loaded UWB-MIMO Antenna System for 3D System-in-Package Applications. *IEEE Access*. 8, 106982–106992; doi: 10.1109/ACCESS.2020.3000134 (2020).

[39] Alam, M. S., Islam, M. T. & Misran, N. A novel compact split ring slotted electromagnetic bandgap structure for microstrip patch antenna performance enhancement. *Prog. Electromagn. Res.*130, 389–409; doi: 10.2528/PIER12060702 (2012).

[40] Abdelaziz, A. & Hamad, E. K. I. Isolation enhancement of 5G multiple-input multiple-output microstrip patch antenna using metamaterials and the theory of characteristic modes. *Int. J. RF Microw. Comput. Eng.* 30, 11, 1–13; 10.1002/mmce.22416 (2020).

[41] Al-Bawri, S. S., Islam, M. T., Shabbir, T., Muhammad, G., Shabiul Islam, M. D. & Wong, H. Y. Hexagonal shaped near zero index (NZI) metamaterial based MIMO antenna for millimeter-wave application. *IEEE Access*. 8, 181003–181013; doi: 10.1109/ACCESS.2020.3028377 (2020).

[42] Jain, A. & Yadav, S. K. Design and analysis of compact 108 element multimode antenna array for massive MIMO base station. *Prog. Electromagn. Res. C*. 61, 179–184; doi: 10.2528/PIERC15110502 (2016).

[43] Al-Bawri, S. S., Islam, M. T., Islam, M. S., Singh, M. J. & Alsaif, H. Massive metamaterial system-loaded MIMO antenna array for 5G base stations. *Sci. Rep.* 12, 1, 1–16; doi: 10.1038/s41598-022-18329-y (2022).

[44] Rahman, M. M., Islam,, M. S., Islam, M. T., Al-Bawri, S. S. & Yong, W. H. Metamaterial-based compact antenna with defected ground structure for 5G and beyond. *Comput. Mater. Contin.* 71, 2, 2383–2399; doi: 10.32604/cmc.2022.022150 (2022).

[45] Li, S., Chen, Z. N., Li, T. , Lin, F. H., Member, S. & Yin, X. Characterization of Metasurface Lens Antenna for Massive MIMO and Multibeam Systems. *IEEE Trans. Antennas Propag.* 68, 3, 1366–1377; doi: 10.1109/TAP.2020.2968849 (2020).

[46] Saurabh, A. K. & Meshram, M. K. Compact sub-6 GHz 5G-multiple-input-multiple-output antenna system with enhanced isolation. *Int. J. RF Microw. Comput. Eng.* 1–11; doi: 10.1002/mmce.22246 (2020).

[47] Vadlamudi, R. & Sriram Kumar, D. Very Novel Design and Mutual Coupling Analysis of a Wideband, Tightly Arranged DP massive MIMO (32T and 32R) Antenna Array for 5G Base Station Application. *2020 IEEE International Students' Conference on Electrical, Electronics and Computer Science, SCEECS 2020*. 2–6;

doi: 10.1109/SCEECS48394.2020.174 (2020).

[48] Temiz, M., Alsusa, E., Danoon, L. & Zhang, Y. On the Impact of Antenna Array Geometry on Indoor Wideband Massive MIMO Networks. *IEEE Trans. Antennas Propag.* 69, 1, 406–416; doi: 10.1109/TAP.2020.3008662 (2021).

[49] Ibrahim, S. K. et al. Compact metamaterial-based single/double-negative/near-zero index resonator for 5G sub-6 GHz wireless applications. *Sci. Rep.* 14, 1, 1–25; doi: 10.1038/s41598-024-63610-x (2024).

[50] Sharawi, M. S., Hassan, A. T. & Khan, M. U. Correlation coefficient calculations for MIMO antenna systems: A comparative study. *Int. J. Microw. Wirel. Technol.* 9, 10, 1991–2004;

doi: 10.1017/S1759078717000903 (2017).